Supporting Information

Electron Diffraction Tomography and X-ray Powder Diffraction on Photoredox Catalyst PDI

Keywords: PDI, XRPD, electron diffraction, DFT-D photoredox-catalysts

Authors: Alexander Bodach,[a] Haishuang Zhao,[b] Nai-Wei Liu,[c] Edith Alig,[a] Georg Manolikakes,[c, d] Ute Kolb[b, e] and Lothar Fink[a*]

*Corresponding author: fink@chemie.uni-frankfurt.de

[a] Institute of Inorganic and Analytical Chemistry, Goethe University Frankfurt am Main, Max-von-Laue-Str. 7, 60438 Frankfurt am Main, Germany-

[b] Institute of Inorganic Chemistry and Analytical Chemistry, Johannes Gutenberg University, Duesbergweg 10-14, 55128 Mainz, Germany-

[c] Institute of Organic Chemistry and Chemical Biology; Goethe University Frankfurt am Main, Max-von-Laue-Str. 7, 60438 Frankfurt am Main, Germany.

[d] Department of Chemistry, TU Kaiserslautern, Erwin-Schrödinger-Str. Geb. 54, 67663 Kaiserslautern, Germany.

[e] Institute of Applied Geosciences, TU Darmstadt, Schnittspahnstraße 9, 64287 Darmstadt, Germany.

Table of Content

1 General Information

1.1 Reactions

Unless otherwise mentioned, all reactions were carried out under an argon atmosphere in flame dried glassware applying standard Schlenk techniques. All yields refer to isolated yields of compounds estimated to be > 95% pure as determined by ^{1}H-NMR.

1.2 Chromatography

Column chromatography was performed with Silica 60 (0.04-0.063 mm, 230-400 mesh) and the specified solvent mixture. Thin layer chromatography was performed on aluminum sheets coated with SiO_2 (TLC silica gel 60 F254). The spots were visualized by ultraviolet light.

1.3 Solvents

Solvents for reactions and column chromatography were obtained from different commercial suppliers in >97% purity and used as received. All anhydrous solvents were purchased from commercial suppliers and stored over MS 4 Å under an atmosphere of argon. Solvents for column chromatography were technical standard.

1.4 Materials

All starting materials, which were obtained from commercial sources and used without further purification.

1.5 NMR spectroscopy

Proton nuclear magnetic resonance spectra (^{1}H NMR), carbon spectra (^{13}C NMR) were recorded at 300 MHz (^{1}H) 75 MHz (^{13}C), respectively. Chemical shifts are reported as δ - values relative to the residual $CDCl_3$ (δ = 7.26 ppm for ^{1}H and δ = 77.16 ppm for ^{13}C). Coupling constants (J) are given in Hz and multiplicities of the signals are abbreviated as follows: d = doublet; dd = doublet of doublets and hept = heptet.

1.7 Mass spectrometry

Mass spectra (MS) were measured using electrospray ionization (ESI) techniques.

2 Synthesis and NMR spectra

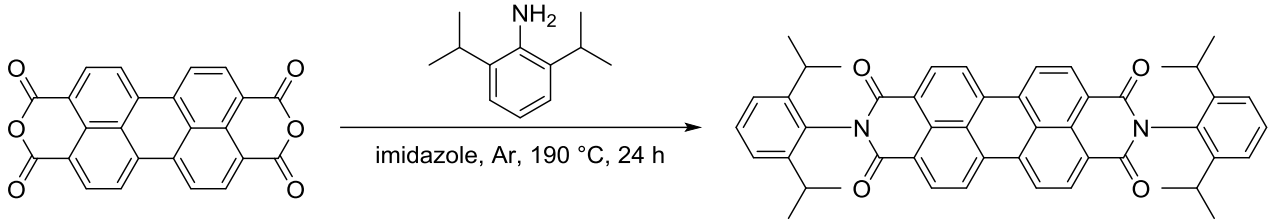

PDI-*i*Pr, 22%

Synthesis: PDI-*i*Pr was synthesized based on a modified procedure by Ghosh *et al.*[1] Perylenetetracarboxylic dianhydride (PTCDA, 4.08 g, 10.2 mmol, 1 Eq), 2,6-diisopropylaniline (8.0 mL, 7.5 g, 42 mmol, 4.2 Eq) and imidazole (30.1 g) were heated to 190°C for 24 h under Ar atmosphere. After cooling to ambient temperature 50 mL HCl (6 M) and 100 mL EtOH were added, suspended in an ultrasonic bath and filtrated. The crude product was dissolved and purified by column chromatography with *n*-hexane/CH_2Cl_2 (1:1 to CH_2Cl_2 only). All orange and green fractions were collected and the solvent was removed under reduced pressure and dried *in vacuo* to yield the red powdery product (1.6 g, 22%).

Analytical data are consistent with the literature.[1]

R_F = 0.5 (CH_2Cl_2)

^{1}H NMR (300 MHz, $CDCl_3$) δ 8.80 (d, J = 8.0 Hz, 4H), 8.75 (d, J = 8.1 Hz, 4H), 7.51 (dd, J = 8.2, 7.3 Hz, 2H), 7.36 (d, J = 7.6 Hz, 4H), 2.76 (hept, J = 6.8 Hz, 4H), 1.19 (d, J = 6.8 Hz, 24H).
^{13}C NMR (75 MHz, $CDCl_3$) δ 163.6, 145.8, 135.2, 132.3, 130.7, 130.3, 129.9, 127.0, 124.3, 123.6, 123.5, 29.4, 24.2.
MS (ESI) m/z calcd. for $C_{48}H_{43}N_2O_4$ $[M+H^+]$ = 711.3; found : 711.3.
Decomposition temperature 475 °C, Fig. S8.

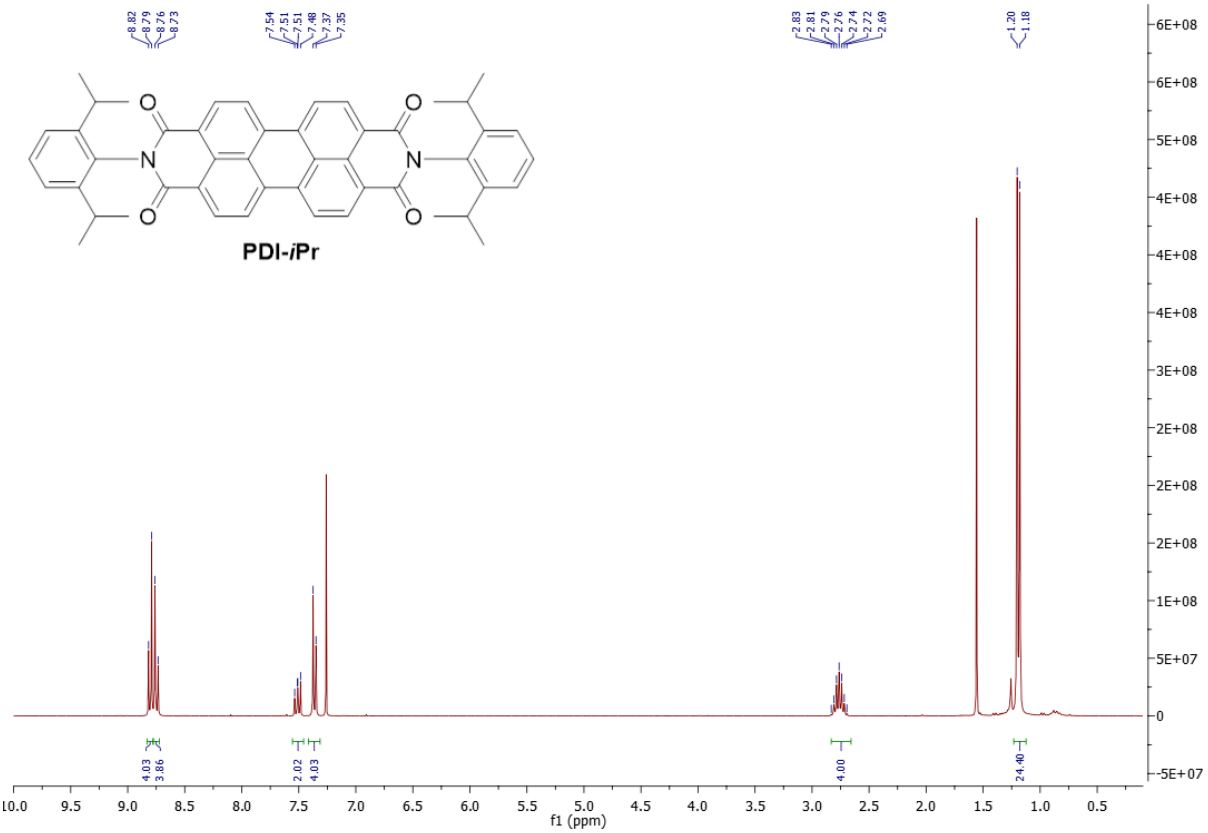

Fig. S1. ^{1}H-NMR spectrum of **PDI-*i*Pr** in $CDCl_3$.

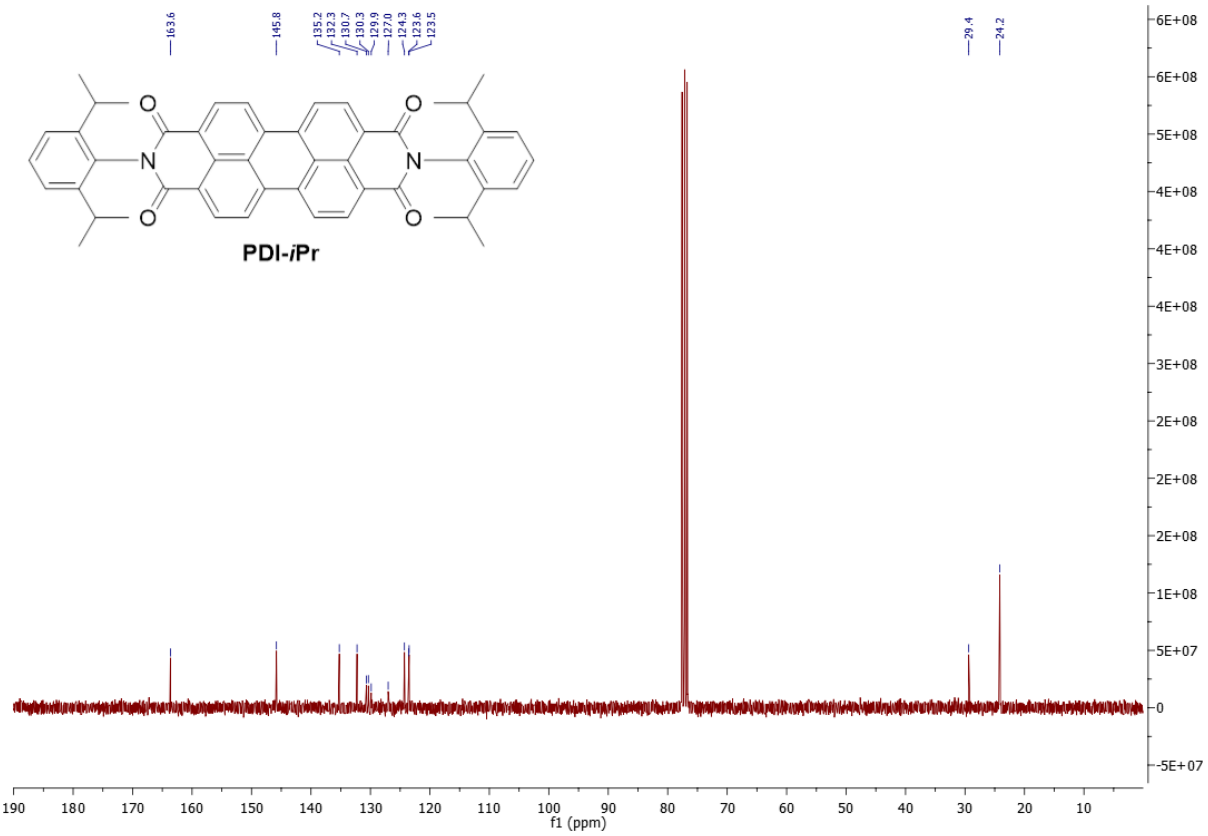

Fig. S2. ^{13}C-NMR spectrum of **PDI-*i*Pr** in $CDCl_3$.

3 Electron diffraction experiments

Measurement As **PDI-*i*Pr** can be dissolved in the common solvents, it is difficult to achieve a suitable dispersion. Therefore 300 mesh Cu TEM grids and sample powder were shook together in a glass. After checking in TEM some crystal particles were adsorbed on the grids used for TEM measurements.

Phase contrast TEM, scanning TEM (STEM), and automated diffraction tomography (ADT) measurements were carried out using a TECNAI F30 S-TWIN transmission electron microscope equipped with a field emission gun and operating at 300 kV. STEM images were collected using a Fischione high-angle annular dark field (HAADF) detector, an example image of CryI can be found in Fig S3. TEM images and nano electron diffraction (NED) patterns were acquired with a 4k x 4k Gatan US4000 CCD camera (Gatan, Pleasanton, USA). In order to increase the stability of sample under the electron beam, the sample was cooled down to about 97 K using a cyro-transfer tomography holder filled with liquid N_2 after insertion into TEM. Electron diffraction data were collected with an automated acquisition module developed for FEI microscopes[2]. A Gatan cryotransfer tomography holder (model 914) with a tilt range of ± 70° was used for electron diffraction data acquisition. A small condenser aperture of 10 μm, weak gun lens and large condenser spot size were used in order to reduce the electron dose rate on the sample. The crystal position was tracked in microprobe STEM mode, and electron diffraction patterns were collected using the above settings. The beam size was set to 100 nm in diameter. In order to reduce dynamic effects, ADT was coupled with precession electron diffraction (PED)[3, 4]NanoMEGAS DigiStar unit. The precession angle of the beam was kept at 1°. ADT tilt series were collected sequentially in a fixed tilt step of 1°. The exposure time for each frame was set to 3 s. Two datasets of different crystals were collected and merged (Tab. S1)

Structure Solution The ADT3D software[4, 5] was used for processing the three-dimensional electron diffraction data yielding unit-cell parameters, space group and reflection intensities. The unit-cell parameters were refined with a Pawley[6] fit against XRPD data. The ab initio structure

solution using direct methods approach implemented in SIR2014[7] was based on the reflection intensities derived from ADT data.

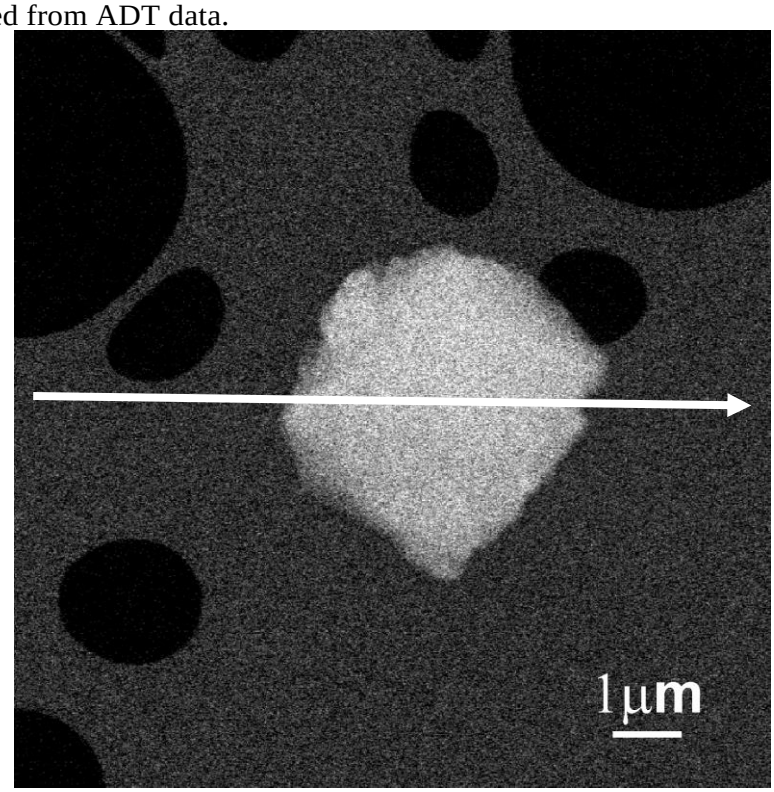

Fig S3. STEM image of Crystal I for ADT measurement. Tilt axis horizontal.

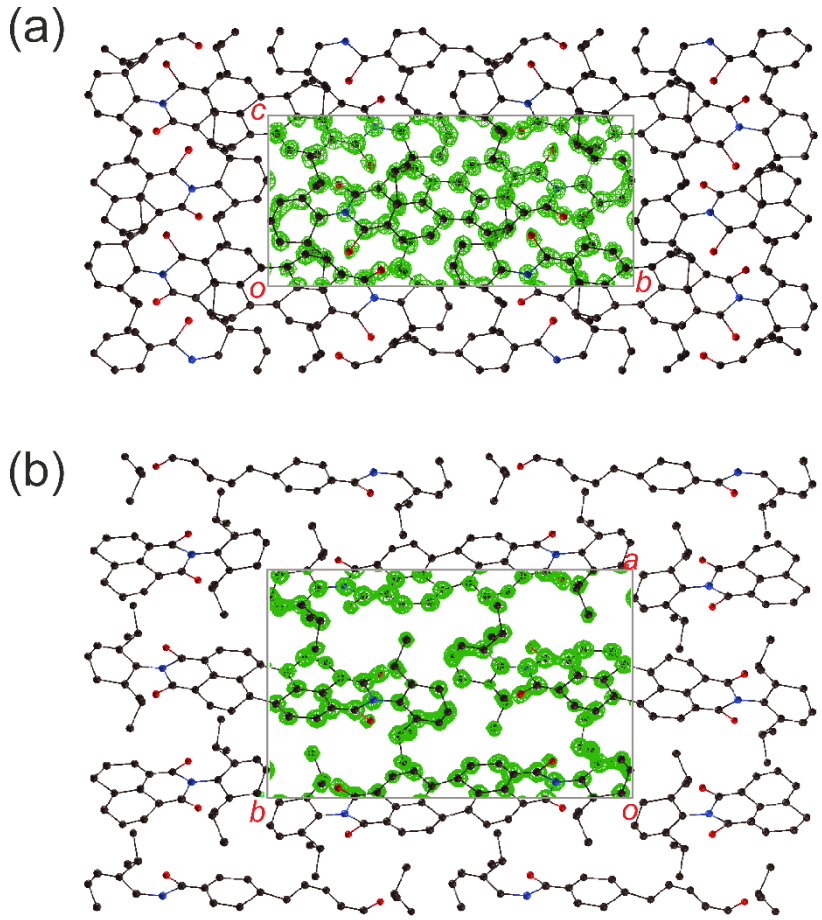

Fig. S4. Potential map of PDI-*i*Pr in Sir2014 derived from ADT data overlaid with the atomic model, viewed in [100] zone for (a) and [001] zone for (b), respectively. The potentials (in green) are set with sigma of 2.8 $e^{-}/Å^{3}$ -. C in black, N in blue and O in red.

Table S1 Experimental parameters of electron diffraction datasets used for structure solution in space group $P2_1/n$.

	Merged data	Unmerged data	
Dataset	CryI + CryII	CryI	CryII
Tilt range (°)		-62/+18	-60/+28
No. of total reflections	7913	4325	4549
No. of independent reflections	2650	1843	1684
Resolution (Å)	0.9	0.9	0.9
Independent reflection coverage (%)	89	62	57
R_{int}	0.266	0.231	0.236
Residual *R* (*SIR2014*)	0.295	0.313	0.309

4 X-ray Powder Diffraction

Measurement The sample consisting of microcrystalline powder was sealed in a borosilicate glass capillary with 0.7 mm diameter. The measurements were carried out in Debye-Scherrer geometry on a STOE STADI P diffractometer equipped with a curved Ge(111) monochromator to produce pure Cu-$K_{\alpha 1}$ (λ = 1.5406 Å) radiation. The spun sample was measured at 2θ angles from 2° to 110° in 0.01° steps. With a measurement time of about one week the data was recorded by a linear position sensitive detector (lin. PSD, STOE, Kr/CH_4) and evaluated with the WINXPow[8] software package.

Indexing and Rietveld Refinement Indexing of the XRPD data with DICVOL[9] and Pawley[6] refinement revealed a monoclinic unit cell with the parameters given in Tab. S2. Z = 2, and Z' = ½ were estimated with Hofmann's volume increments.[10]

Rietveld[11, 12] refinement of the crystal structure was carried out with the program TOPAS.[13, 14]perylene pseudo-atoms were used. The isotropic atomic displacement parameters (*ADPs*) were refined separately for the alkyl, phenyl and perylene system, while the *ADP* for hydrogen was constrained to be 1.2 times the alkyl *ADP*. Within the XRPD data the 2θ range of 10.25° to 10.55° was excluded, due to an artificial signal (Fig. S5).

For validation purposes an additional low-temperature measurement was carried out within a shorter time period by applying an Oxford Cryostream 700Plus (Oxford Cryosystems). The Rietveld refinement converged with sufficient quality criteria and a smooth difference curve without conspicuity with respect to the data quality (Table S2 and Fig. S6)

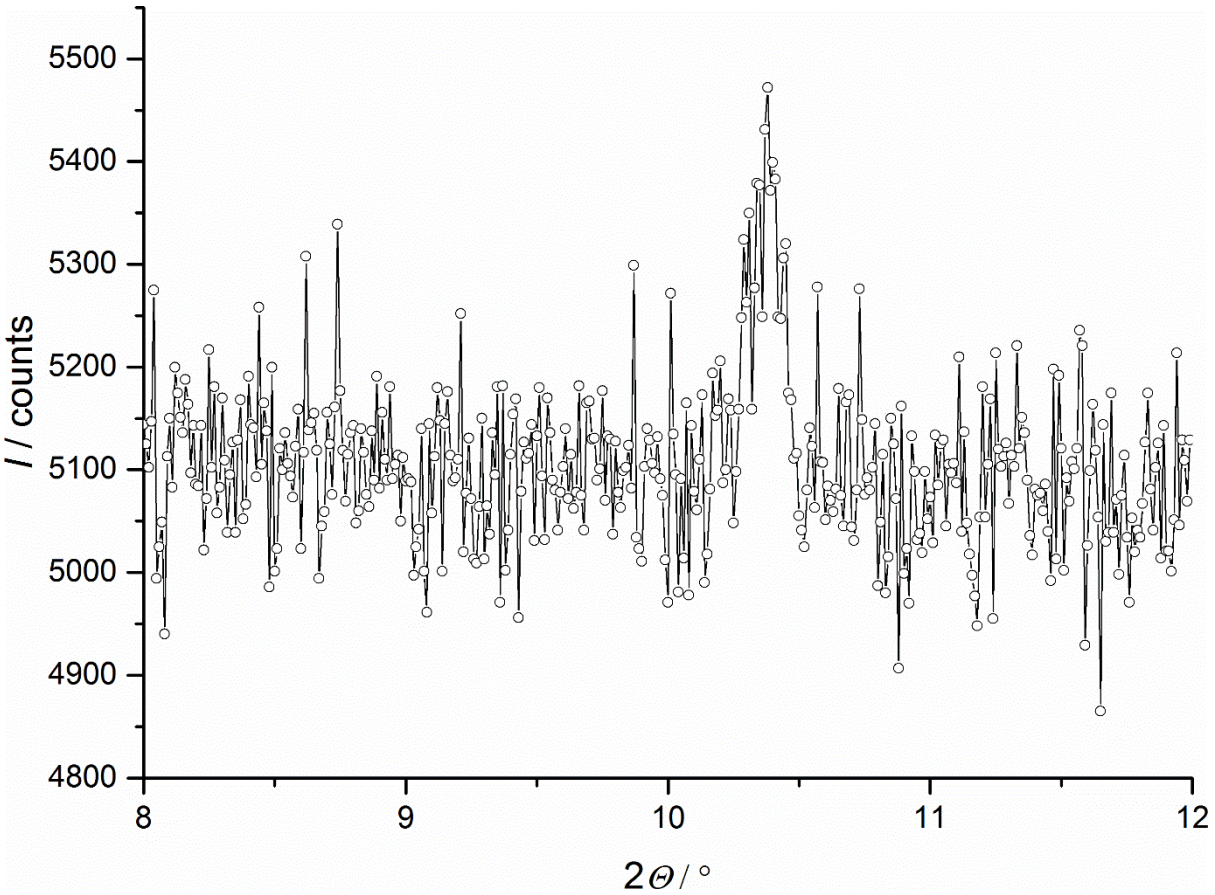

Fig. S5. XRPD measurement of an empty capillary shows a small artificial signal.

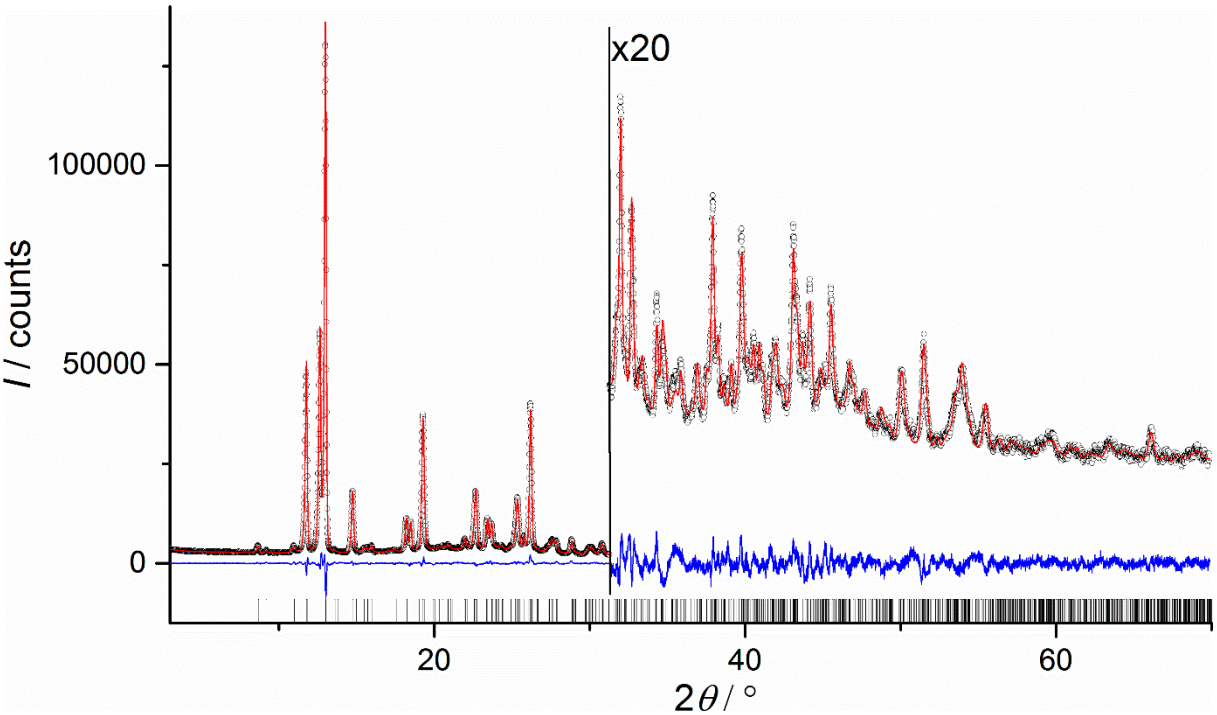

Fig. S6. Rietveld-Plot of the refinement of the crystal structure of **PDI-*i*Pr** (low-temperature data), I_{exp} (black circles), I_{calc} (red line), I_{exp}-I_{calc} (blue line), positions of Bragg reflections (tick marks).

5 DFT-D calculations

Based on our previous described procedures[15, 16] we used an adjusted standard procedure for plane-wave DFT-D calculations with program CASTEP[17]. Perdew-Burke-Ernzerhof (PBE)[18] basis set and "ultrasoft" pseudo potentials were used. Grimme D2[19] as well as Tkatchenko-Scheffler[20] dispersion corrections were applied with a cut-off energy of 520 eV. Examples are supplied below. According to van de Streek and Neumann *root-mean-square-cartesian-displacement* (RMSCD) parameters were calculated.[21, 22] The overlays of the experimental and calculated crystal structure are given in Fig. S7 and S8, respectively.

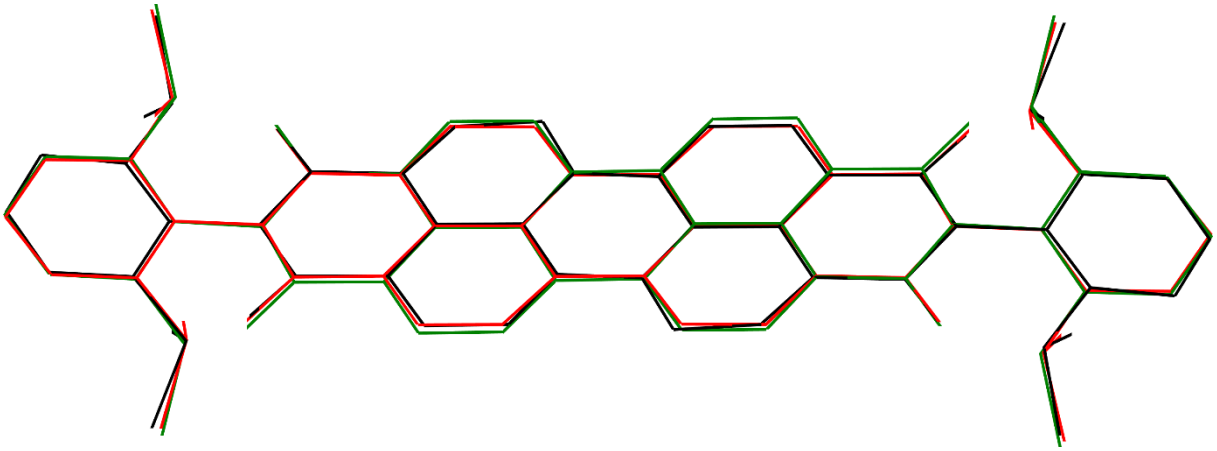

Fig. S7. Overlay of the **PDI-*i*Pr** molecules, experimental from XRPD data (black), calculated with fixed unit cell (TS dispersion correction, red), calculated with optimized unit cell (TS dispersion correction, green)

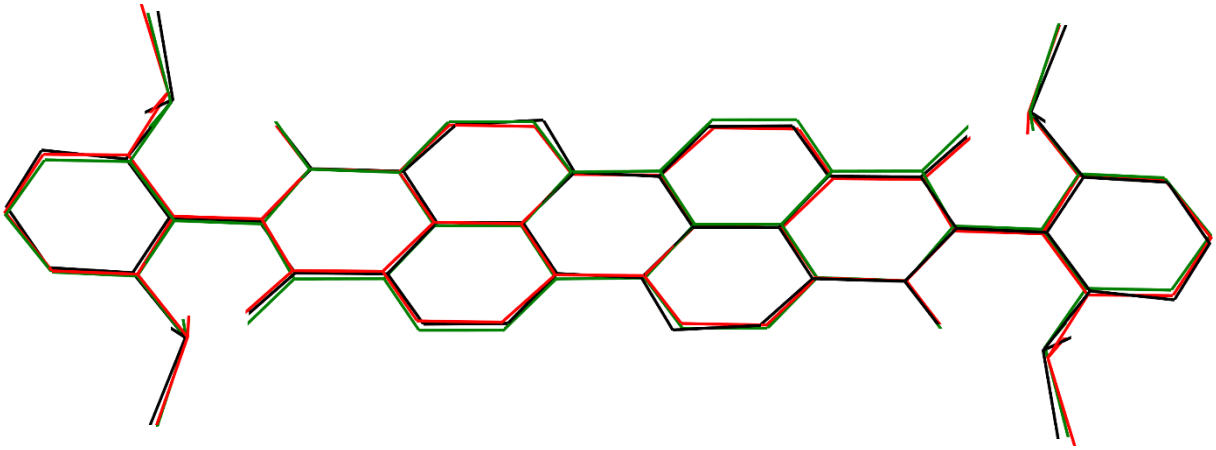

Fig. S8. Overlay of the **PDI-*i*Pr** molecules, experimental from XRPD data (black), calculated with fixed unit cell (D2 dispersion correction, red), calculated with optimized unit cell (D2 dispersion correction, green)

Example: fixed unit cell and Tkatchenko-Scheffler dispersion correction

comment : fixed unit cell
task : GeometryOptimization
xc_functional : PBE
sedc_apply : true
sedc_scheme : TS
spin_polarized : false
opt_strategy : Speed
page_wvfns : 0
cut_off_energy : 520.000000000000000
grid_scale : 1.750000000000000
fine_grid_scale : 2.100000000000000
finite_basis_corr : 2
finite_basis_npoints 3
elec_energy_tol : 1.000000000000000e-006
max_scf_cycles : 200
fix_occupancy : true
metals_method : dm
mixing_scheme : Pulay
mix_charge_amp : 0.500000000000000
mix_charge_gmax : 1.500000000000000
mix_history_length : 20
nextra_bands : 0
geom_energy_tol : 1.000000000000000e-005
geom_force_tol : 0.030000000000000
geom_stress_tol : 0.050000000000000
geom_disp_tol : 1.000000000000000e-003
geom_max_iter : 2000
geom_method : Delocalized
fixed_npw : false
calculate_ELF : false
calculate_stress : false
popn_calculate : false
calculate_hirshfeld : false
calculate_densdiff : false
pdos_calculate_weights : false
num_dump_cycles : 0

Example: optimized unit cell and Tkatchenko-Scheffler dispersion correction

comment : optimized unit cell
task : GeometryOptimization
xc_functional : PBE
sedc_apply : true
sedc_scheme : TS
spin_polarized : false
opt_strategy : Speed
page_wvfns : 0
cut_off_energy : 520.000000000000000
grid_scale : 1.750000000000000
fine_grid_scale : 2.100000000000000
finite_basis_corr : 2
finite_basis_npoints : 3
elec_energy_tol : 1.000000000000000e-006
max_scf_cycles : 200
fix_occupancy : true
metals_method : dm
mixing_scheme : Pulay
mix_charge_amp : 0.500000000000000
mix_charge_gmax : 1.500000000000000
mix_history_length : 20
nextra_bands : 0
geom_energy_tol : 1.000000000000000e-005
geom_force_tol : 0.030000000000000
geom_stress_tol : 0.050000000000000
geom_disp_tol : 1.000000000000000e-003
geom_max_iter : 2000
geom_method : BFGS
fixed_npw : false
geom_modulus_est : 25.000000000000000 GPa
calculate_ELF : false
calculate_stress : true
popn_calculate : false
calculate_hirshfeld : false
calculate_densdiff : false
pdos_calculate_weights : false
num_dump_cycles : 0

6 Differential thermal analysis and thermogravimetry (DTA-TG)

DTA-TG Measurements were performed on a SETARAM (TGA 92) device. The sample was transferred to a 100 µL Al_2O_3 crucible and measured under argon atmosphere with a heating rate of 10 K/min.

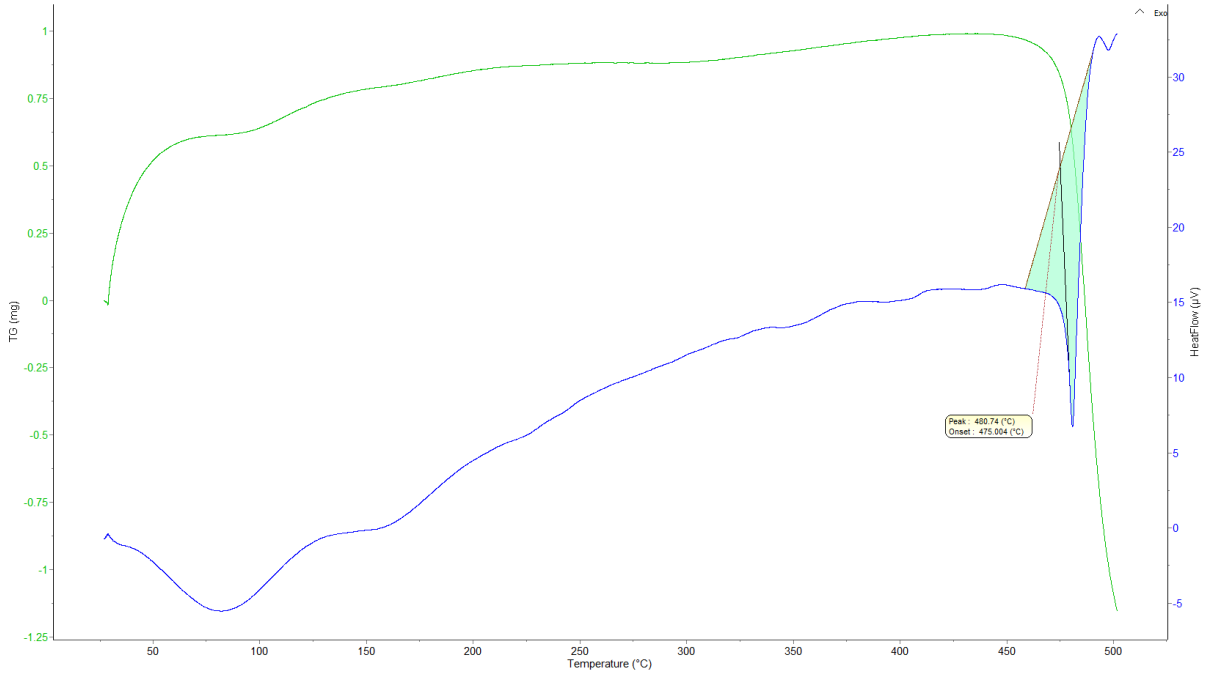

Fig. S9. DTA-TG measurement of **PDI-*i*Pr** exhibits decomposition above 470°C.

7 Density determination by pycnometry

First the density of *n*-hexane was determined, classically. About 20 mg **PDI-*i*Pr** were weighted and the density determined in 1mL n-hexane by pycnometry. Both densities were determined twice and averaged, the *esd* was expected to be the absolute deviation from the average. D_{exp} = 1.13(1) Mg·m^{-3}.

8 Crystallographic Data

Table S2: Selected crystallographic data of PDI-*i*Pr .

Parameter	**PDI-*i*Pr**	**PDI-*i*Pr (low-temperature)**
Formula	$C_{48}H_{42}N_2O_4$	$C_{48}H_{42}N_2O_4$
MW /g·mol^{-1}	710.87	710.87
Space group (*No.*)	$P2_1/n$ (14)	$P2_1/n$ (14)
a /Å	12.0344(2) 19.14632(25)	12.0476(2)
b /Å	19.1463(3)	19.1589(4)
c /Å	9.0158(2)	8.9033(4)
ß /°	95.8888(8)	95.936(1)
V /Å^3	2066.40(5)	2040.04(6)
Z / *Z'*	2 / ½	2 / ½
D_{calc} /Mg·m^{-3}	1.142	1.156
Radiation type	Cu-$K_{\alpha1}$	Cu-$K_{\alpha1}$
λ /Å	1.5406	1.5406
$2\theta_{max}$ /°	110	70
R_p /%	2.0	2.9
R_p' /%	6.4	6.9
R_{wp} / /%	2.5	3.6
R_{wp}' /%	8.9	8.9
R_{exp} /%	1.6	1.9
R_{exp}' /%	5.9	4.5
gof	1.6	2.0
RMSCD (TS-fix) /Å	0.11	-
RMSCD (TS-free) /Å	0.13	-
RMSCD (D2-fix) /Å	0.15	-
RMSCD (D2-free) /Å	0.17	-

R_p', R_{wp}' and R_{exp}' according to TOPAS[13, 14]

9 References

1. I. Ghosh, T. Ghosh, J. I. Bardagi and B. König, *Science*, 2014, **346**, 725-728.
2. U. Kolb, T. Gorelik, C. Kübel, M. Otten and D. Hubert, *Ultramicroscopy*, 2007, **107**, 507-513.
3. R. Vincent and P. Midgley, *Ultramicroscopy*, 1994, **53**, 271-282.
4. E. Mugnaioli, T. Gorelik and U. Kolb, *Ultramicroscopy*, 2009, **109**, 758-765.
5. U. Kolb, T. Gorelik and M. Otten, *Ultramicroscopy*, 2008, **108**, 763-772.
6. G. Pawley, *J. Appl. Crystallogr.*, 1981, **14**, 357-361.
7. M. C. Burla, R. Caliandro, B. Carrozzini, G. L. Cascarano, C. Cuocci, C. Giacovazzo, M. Mallamo, A. Mazzone and G. Polidori, *J. Appl. Crystallogr.*, 2015, **48**, 306-309.
8. WinXPOW, *Darmstadt: Stoe & Cie GmbH*, 2010, Version 3.03.
9. A. Boultif and D. Louër, *J. Appl. Crystallogr.*, 2004, **37**, 724–731.
10. D. W. Hofmann, *Acta Crystallogr. B.*, 2002, **58**, 489-493.
11. H. Rietveld, *J. Appl. Crystallogr.*, 1969, **2**, 65–71.
12. H. M. Rietveld, *Acta Cryst.*, 1967, **22**, 151–152.
13. A. A. Coelho, *TOPAS-Academic V4.2, Software, Brisbane Australia*, 2009.
14. TOPAS, *Karlsruhe, Germany*, 2008.
15. L. Fink, K. Samigullin, A. Bodach, E. Alig, M. Wagner and H.-W. Lerner, *Z. Anorg. Allg. Chem*, 2016, **642**, 282–287.
16. C. Partes, A. Bodach, E. Alig and L. Fink, *Z. Kristallogr. Cryst. Mater.*, 2016, **231**, 709–714.
17. S. J. Clark, M. D. Segall, C. J. Pickard, P. J. Hasnip, M. I. Probert, K. Refson and M. C. Payne, *Z. Kristallogr. Cryst. Mater.*, 2005, **220**, 567-570.
18. J. P. Perdew, K. Burke and M. Ernzerhof, *Phys. Rev. Lett.*, 1996, **77**, 3865.
19. S. Grimme, *J. Comput. Chem.*, 2006, **27**, 1787-1799.
20. A. Tkatchenko and M. Scheffler, *Phys. Rev. Lett.*, 2009, **102**, 073005.
21. J. van de Streek and M. A. Neumann, *Acta Crystallogr. B.*, 2010, **66**, 544–558.
22. J. van de Streek and M. A. Neumann, *Acta Crystallogr. B.*, 2014, **70**, 1020–1032.